

# Hyperfine splitting of [Al VI] 3.66 $\mu\text{m}$ and the Al isotopic ratio

Simon Casassus<sup>1</sup>, Pete Storey<sup>2</sup>, Mike Barlow<sup>2</sup>, Pat Roche<sup>3</sup>

<sup>1</sup> U. de Chile, <sup>2</sup> UCL, <sup>3</sup> Oxford  
simon@das.uchile.cl

## Abstract

Spectra of [Al VI] 3.66 $\mu\text{m}$   $^3P_2 \leftarrow ^3P_1$  in the coronal region of PN NGC 6302, obtained with Phoenix on Gemini-South at resolving powers of up to 75000, resolve the line into five hyperfine components separated by 20 to 60 km s<sup>-1</sup> due to the coupling of the  $I = 5/2$  nuclear spin of  $^{27}\text{Al}$  with the total electronic angular momentum  $J$ .

$^{26}\text{Al}$  has a different nuclear spin of  $I = 5$ , and a different hyperfine structure (HFS), which allows us to place a  $3\sigma$  upper limit on the  $^{26}\text{Al}/^{27}\text{Al}$  ratio of 1/33.

We measure the HFS magnetic-dipole coupling constants for [Al VI], and provide the first observational estimates of atomic electric-quadrupole HFS coupling constants.

## 1. Introduction

### 1.1 The $^{26}\text{Al}$ problem

The 1.8 MeV gamma-ray emission due to the decay of  $^{26}\text{Al}$  into  $^{26}\text{Mg}$  has been the object of extensive surveys: with a half-life of 7.2  $10^5$  yr,  $^{26}\text{Al}$  is a signpost of recent nucleosynthesis.

Line emission at 1.8 MeV from the diffuse ISM is consistent with an  $^{26}\text{Al}$  source in either AGB stars (Forestini et al. 1991, A&A, 252, 597), novae, supernovae, Wolf-Rayet stars (Prantzos 2004, MNRAS, 420, 1033) or from cosmic-ray collisions in molecular clouds (Clayton 1994, Nature, 368, 222) through  $^{26}\text{Mg}^*(\text{H},\text{n})^{26}\text{Al}$ .

SiC inclusions in the Murchison meteorite have  $^{26}\text{Mg}$  levels indicative of  $^{26}\text{Al}/^{27}\text{Al} \approx 1$  in the SiC grains of the pre-solar nebula (with an AGB origin).

But the  $^{26}\text{Al}/^{27}\text{Al}$  isotopic abundance ratio has never been measured in any astrophysical source.

The only available upper limit in any specific object is that of Banerjee et al. (2004, ApJL, 610, 29), who observed the (2-0) vibronic bands of the A-X system in AIO at 1.5  $\mu\text{m}$  in the nova-like variable V4332 Sgr, and reported an upper limit of  $\sim 1/10$ .

### 1.2 Hyperfine structure

The interaction between the electronic wave-function and a non-zero nuclear magnetic dipole splits a fine-structure level  $\{L, J\}$  into hyperfine levels. The electric-quadrupole corrections to the electric field introduce an additional correction, which is neglected in photospheric model line profiles, but which dominates over magnetic dipole HFS in molecules.

While hyperfine transitions are common in the radio range, at shorter wavelengths atomic hyperfine structure (HFS) has seldom been resolved in emission.

The first detection of atomic HFS in emission, aside from the 21 cm H I line, is to our knowledge the observation of resolved HFS in  $^{13}\text{C II}$  157.8 $\mu\text{m}$   $^2P_{1/2} \leftarrow ^2P_{3/2}$  by Boreiko et al. (1988, ApJ, 325, L47). Kelly & Lacy (1995, ApJL, 454, 161) identified multiple components in [Na IV] 9.0 $\mu\text{m}$  with the hyperfine splitting of  $^3P_2 \leftarrow ^3P_1$ .

## 2. Phoenix observations of NGC 6302

We observed NGC 6302 with Phoenix on Gemini South on 5 nights of May and July 2003. Fig. 1 shows the slit position. Typical integration times in the [Al VI] settings were 1h-2h on-source for each night, but the noise level largely reflects the weather conditions. The seeing has a direct impact on the resolution of the spectra, by convolving the emission in the slit with neighbouring emission from the expanding nebula.

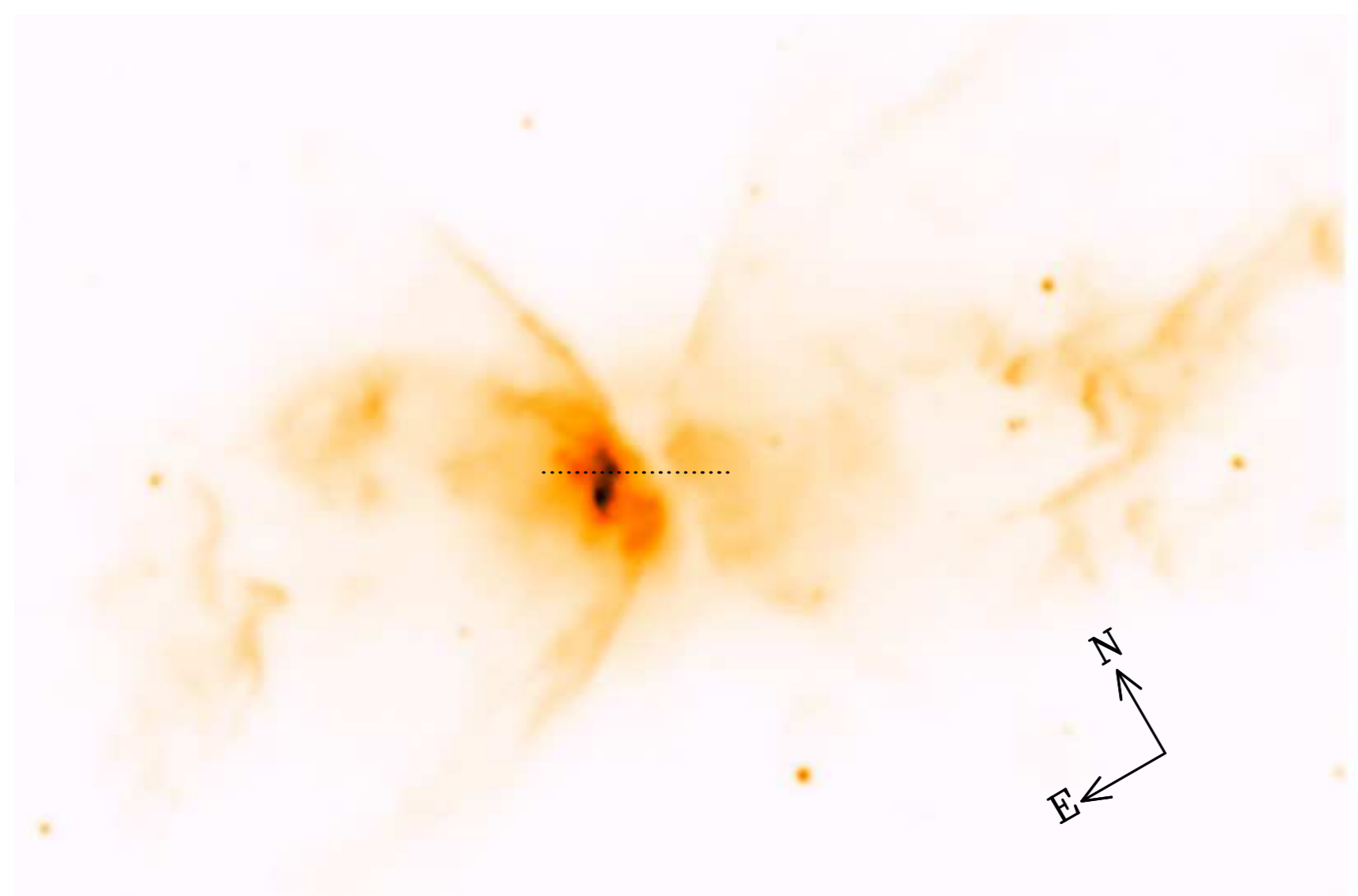


Figure 1: Overlay of the Phoenix 14'' slit on the R-band Gemini acquisition image.

The resulting position-velocity frames are shown in Fig. 2, after subtraction of a small level of continuum nebular emission. There are at least four emission features observed

near the [Al VI] wavelength given by Casassus et al. (2000, MNRAS, 314, 657) of 3.659  $\mu\text{m}$ , with similar position-velocity structures. The night of July 30<sup>th</sup> has the best line contrast, even though we used the widest slit, which reflects a good seeing.

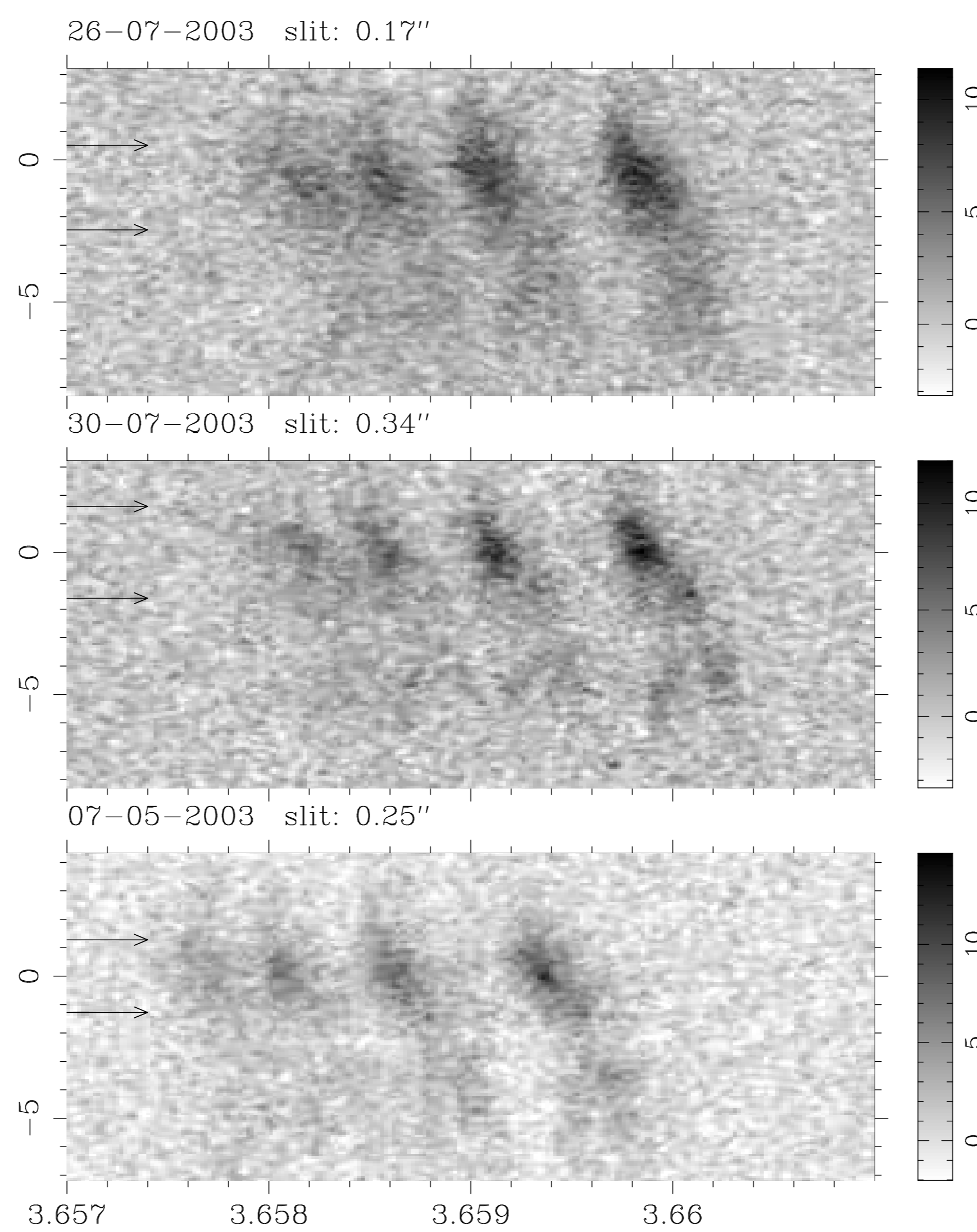


Figure 2: Reduced Phoenix detector array. Intensity in units of  $1\sigma$  noise. x-axis is wavelength in microns, y-axis is offset along the slit in arcsec. The y-axis increases towards the East. The horizontal arrows limit the optimal extraction aperture.

## 3. Model line profiles

We fit the [Al VI] line profile  $F_\lambda$  with a parametrised model, consisting of 2 Gaussians per hyperfine component for both isotopes.  $^{27}\text{Al}/^{26}\text{Al}$  is a free parameter. The hyperfine energy levels are given by

$$\Delta E(L, J, F, I) = \frac{hA_{L,J}}{2}K + hB_{L,J} \left[ K(K+1) - \frac{4}{3}I(I+1)J(J+1) \right], \quad (1)$$

where

$$K = F(F+1) - I(I+1) - J(J+1), \quad (2)$$

and where  $A_{L,J}$  and  $B_{L,J}$  are the magnetic dipole and electric quadrupole coupling constants. The relative intensities  $S(\{J_1, F_1\}, \{J_2, F_2\})$  of each hyperfine component  $\{I, J_1, F_1\} \leftarrow \{I, J_2, F_2\}$  can be derived from

$$S(\{I, J_1, F_1\}, \{I, J_2, F_2\}) = (2F_1+1)(2F_2+1) \left\{ \frac{F_2 F_1}{J_1 J_2} \right\}^2, \quad (3)$$

with the selection rule:

$$|F_1 - F_2| \leq 1 \leq F_1 + F_2, \quad (4)$$

where  $\{ \}$  is the six- $j$  symbol. We obtain

$$R_{\text{iso}} < \langle R_{\text{iso}} \rangle + 3\sigma = 3.0 \cdot 10^{-2},$$

or  $^{27}\text{Al}/^{26}\text{Al} < 1/33$ .

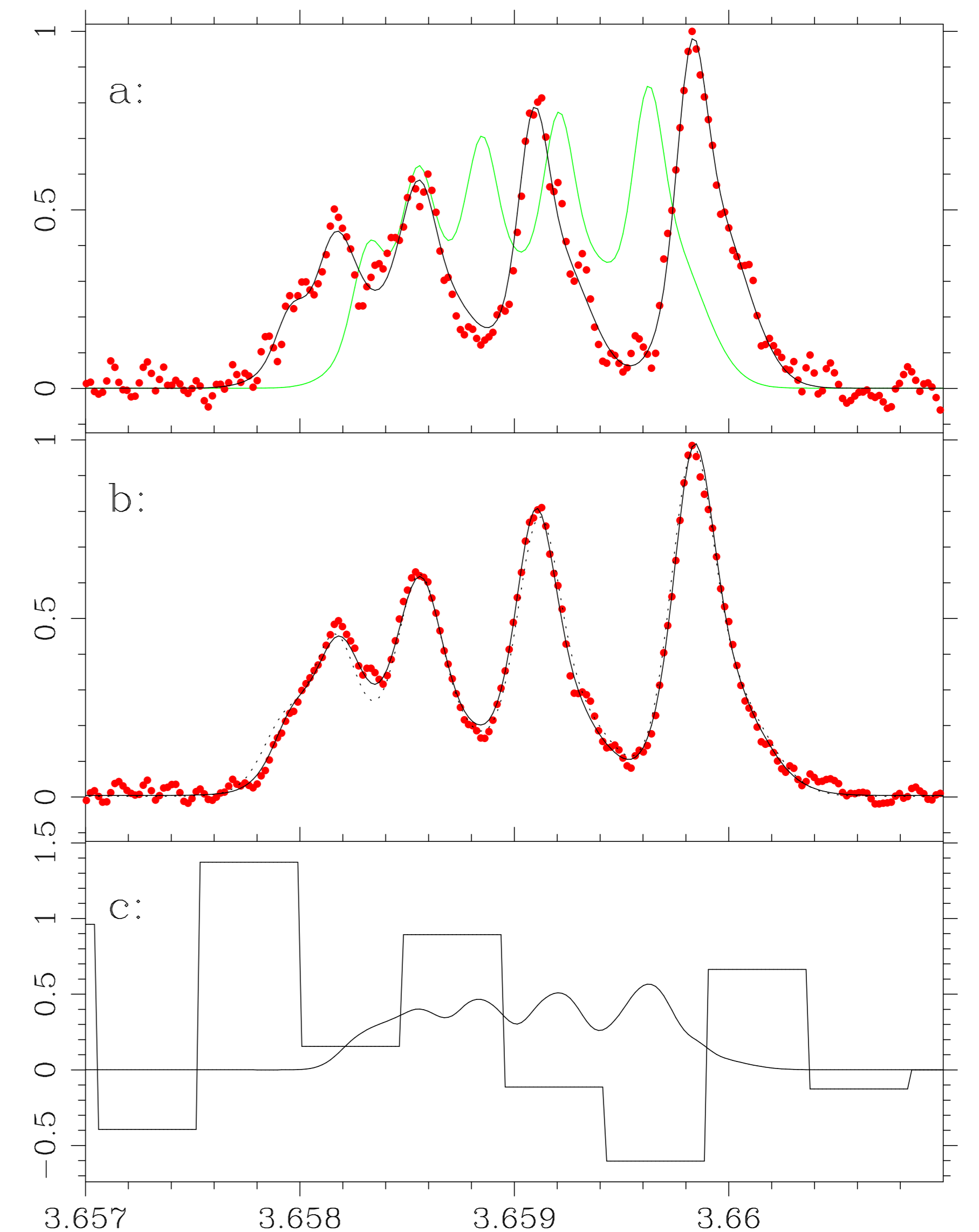


Figure 3: a) Points: collapsed spectrum of [Al VI] from 30-06-2003, with the optimal extraction aperture. Solid line: the best fit with two Gaussians per component, without contribution from  $^{26}\text{Al}$ . Grey solid line: the profile of  $^{26}\text{Al}$ , had it been present at a level giving an isotope ratio of 1. b) Points: coadded spectrum. Solid-line: combined model. Dotted-line: combined model without electric-quadrupole hyperfine splitting. c) Histogram: binned residuals, excluding the  $^{26}\text{Al}$  fits. Solid line: combined  $^{26}\text{Al}$  fit.

## 4. Discussion

### 4.1 AGB stars as $^{26}\text{Al}$ producers

We are short of quantifying  $^{26}\text{Al}$  production in AGB stars through  $^{25}\text{Mg}(p,\gamma)^{26}\text{Al}$ . The expected isotopic ratio at the tip of the AGB is at most 1/37, from the ratio of the  $^{26}\text{Al}$  and  $^{27}\text{Al}$  yields in the 6  $M_\odot$  models of Forestini & Charbonnel (1997, A&AS, 123, 241).

### 4.2 An extension to other targets?

Fig. 4 shows mock spectra for three expanding velocities, with velocity dispersions of  $\sigma = 10, 20, 30$  km s<sup>-1</sup>. Limiting expansion velocity is  $\sim 100$  km/s FWHM, depending on S/N. Allowed objects are high-excitation PNe and symbiotic stars.

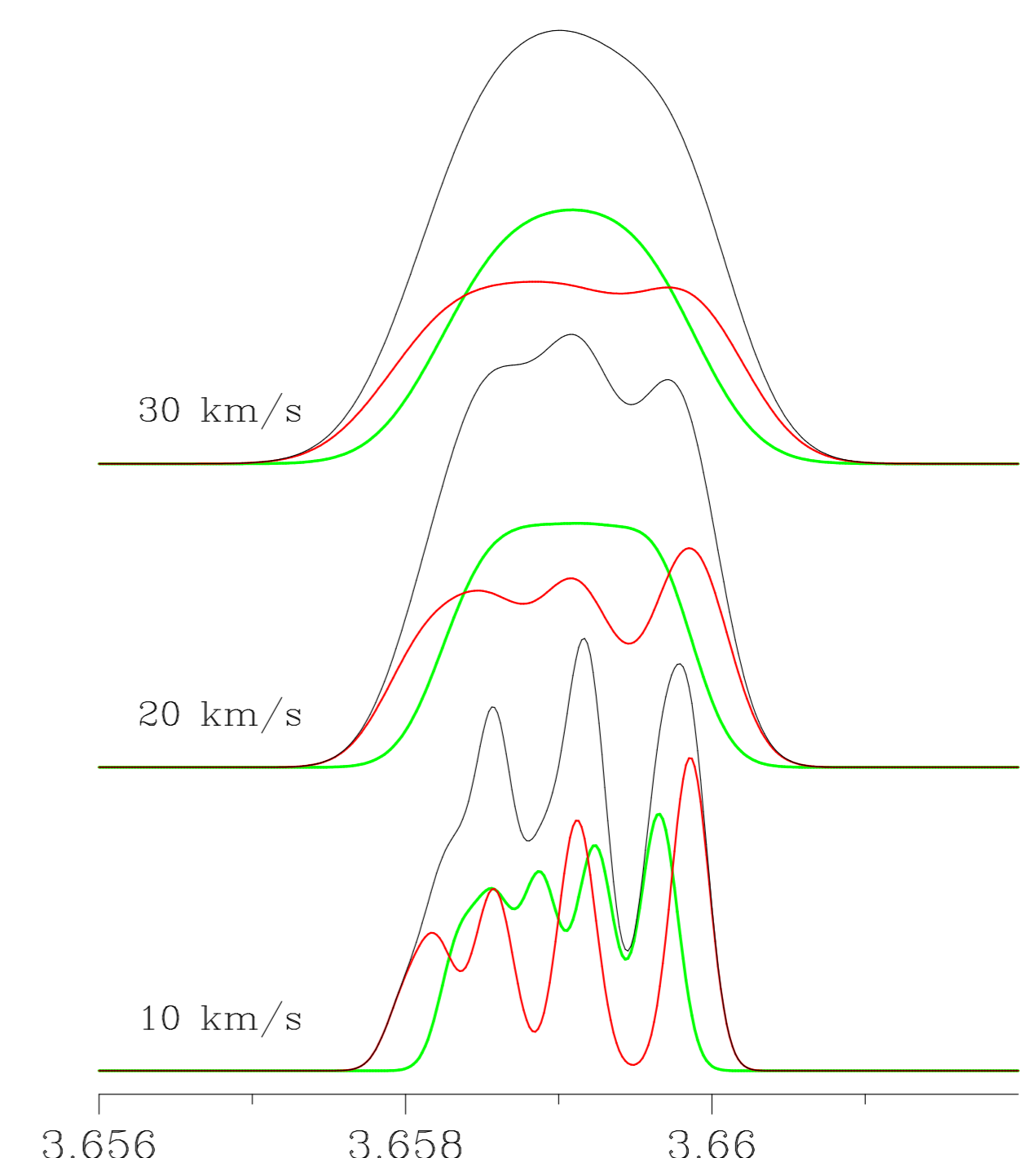


Figure 4: Mock spectra for 3 velocity dispersions

## 5. Conclusions

We obtained the most stringent upper limit on  $^{26}\text{Al}$  production in any astrophysical source, slightly short of constraining AGB stars as sources of  $^{26}\text{Al}$ . The Phoenix spectra allowed: the (difficult) measurement of atomic magnetic-dipole HFS coupling ( $A$ ) constant, and the first-time measurement of atomic electric-quadrupole coupling ( $B$ ) constants in any astrophysical sources. The  $B$  HFS coupling constants lift a statistical bias that affects the  $A$  constants; their inclusion improves the significance of the fits. The accuracy of the magnetic-dipole measurement surpasses the theory by a factor of  $\sim 3$ .